REVIEW ARTICLE

Neoplasia • Vol. 2, Nos. 1–2, January-April 2000, pp. 9–25 9

www.nature.com/neo

Optical Coherence Tomography: An Emerging Technology for Biomedical Imaging and Optical Biopsy[1]

James G. Fujimoto, Costas Pitris*†, Stephen A. Boppart*† and Mark E. Brezinski‡*

*Department of Electrical Engineering and Computer Science, and Research Laboratory of Electronics, Massachusetts Institute of Technology, Cambridge, MA; †Division of Health Sciences and Technology, Harvard Medical School, Boston, MA; ‡Department of Medicine and Cardiac Unit, Harvard Medical School, and Massachusetts General Hospital, Boston, MA

Abstract

Optical coherence tomography (OCT) is an emerging technology for performing high-resolution cross-sectional imaging. OCT is analogous to ultrasound imaging, except that it uses light instead of sound. OCT can provide cross-sectional images of tissue structure on the micron scale *in situ* and in real time. Using OCT in combination with catheters and endoscopes enables high-resolution intraluminal imaging of organ systems. OCT can function as a type of optical biopsy and is a powerful imaging technology for medical diagnostics because unlike conventional histopathology which requires removal of a tissue specimen and processing for microscopic examination, OCT can provide images of tissue *in situ* and in real time. OCT can be used where standard excisional biopsy is hazardous or impossible, to reduce sampling errors associated with excisional biopsy, and to guide interventional procedures. In this paper, we review OCT technology and describe its potential biomedical and clinical applications. *Neoplasia* (2000) **2**, 9–25.

Keywords: biopsy, imaging, OCT, optical imaging, optical coherence tomography, tomography.

Introduction

Optical coherence tomography (OCT) is a fundamentally new type of optical imaging modality. OCT performs high-resolution, cross-sectional tomographic imaging of the internal microstructure in materials and biologic systems by measuring backscattered or backreflected light. OCT images are two-dimensional data sets which represent the optical backscattering in a cross-sectional plane through the tissue. Image resolutions of 1 to 15 μm can be achieved one to two orders of magnitude higher than conventional ultrasound. Imaging can be performed *in situ* and in real time. The unique features of this technology enable a broad range of research and clinical applications. This review article provides an overview of OCT technology, its background, and its potential biomedical and clinical applications.

OCT, imaging the internal cross-sectional microstructure of tissues using measurements of optical backscattering or backreflection, was first demonstrated in 1991 [1]. OCT imaging was performed *in vitro* in the human retina and in atherosclerotic plaque as examples of imaging in transparent, weakly scattering media and nontransparent, highly scattering media. OCT was initially applied for imaging in the eye and, to date, OCT has had the largest clinical impact in ophthalmology. The first *in vivo* tomograms of the human optic disc and macula were demonstrated in 1993 [2,3]. OCT enables the noncontact, noninvasive imaging of the anterior eye as well as imaging of morphologic features of the human retina including the fovea and optic disc [4–7]. Working in collaboration with the New England Eye Center, our group has examined over 10,000 patients to date. The technology was transferred to industry and introduced commercially for ophthalmic diagnostics in 1996 (Humphrey Systems, Dublin, CA). Numerous clinical studies have been performed by many groups in the last several years.

More recently, advances in OCT technology have made it possible to image nontransparent tissues, thus enabling OCT to be applied in a wide range of medical specialties [8–11]. Imaging depth is limited by optical attenuation from tissue scattering and absorption. However, imaging up to 2 to 3 mm deep can be achieved in most tissues. This is the same scale as that typically imaged by conventional biopsy and histology. Although imaging depths are not as deep as with ultrasound, the resolution of OCT is more than 10 to 100 times finer than standard clinical ultrasound. OCT has been applied *in vitro* to image arterial pathology and can differentiate plaque morphologies [11,12]. Imaging studies have also been performed *in vitro* to investigate applications in dermatology, gastroenterology, urology, gynecology, surgery, neurosurgery, and rheumatology [9,13–28]. OCT has also been applied *in vivo* to image developing biologic specimens (*Xenopus laevis, Rana pipiens*, and *Brachyodanio rerio* tadpoles and embryos) [29–31]. For applications in deve-

Address all correspondence to: Dr. James G. Fujimoto, Massachusettes Institute of Technology and Computer Science and Research Laboratory of Electronics, Cambridge, MA, 02139.

[1]This research is supported in part by the National Institutes of Health, Contracts NIH-9-RO1-CA75289-02, NIH-9-RO1-EY11289-13, NIH-RO1-AR44812-02, NIH-1-R29-HL55686-02A1, the Office of Naval Research Medical Free Electron Laser Program, Contract N000014-97-1-1066, and the Whittaker Foundation Contract 96-0205. Dr. Boppart was supported by the Air Force Palace Knight program.
Received 24 August 1999; Accepted 5 November 1999.

lopmental biology, OCT is of interest because it allows repeated imaging of developing morphology without the need to sacrifice specimens.

Numerous developments in OCT technology have also been made. High-speed real-time OCT imaging has been demonstrated with acquisition rates of several frames per second [15,32,33]. High-resolution and ultrahigh-resolution OCT imaging have been demonstrated using novel laser light sources and axial resolutions as high as 1 μm have been achieved [34–36]. Cellular level OCT imaging has recently been demonstrated in developmental biology specimens [37]. OCT has been interfaced with catheters, endoscopes, and laparoscopes which permit internal body imaging [38,39]. Catheter and endoscope OCT imaging of the gastrointestinal, pulmonary, and urinary tracts as well as arterial imaging has been demonstrated *in vivo* in an animal model [15,28,40]. Preliminary endoscopic OCT studies in human subjects have been reported [41,42]. Preliminary clinical studies are currently being performed by many research groups.

In general, there are three types of clinical scenarios where we believe that OCT could have important applications: 1) where conventional excisional biopsy is hazardous or impossible, 2) where conventional biopsy has an unacceptably high false negative rate because of sampling errors, and 3) For guidance of surgical interventional procedures. In this manuscript, we review the fundamental concepts of OCT technology and discuss potential applications to biomedical research and clinical medicine.

Optical Coherence Tomography Compared to Ultrasound

OCT imaging is somewhat analogous to ultrasound B mode imaging except that it uses light instead of sound. Because of the analogy between OCT and ultrasound, it is helpful to begin by considering the factors which govern OCT imaging compared to ultrasound imaging. To perform cross-sectional or tomographic imaging, it is first necessary to measure the internal structure of materials or tissues along a single axial or longitudinal dimension. In OCT, the first step in constructing a tomographic image is the measurement of axial distance or range information within the material or tissue. There are several different embodiments of OCT, but in essence OCT performs imaging by measuring the echo time delay and intensity of backscattered or backreflected light from internal microstructure in materials or tissues. OCT images are a two-dimensional or three-dimensional data set which represent differences in optical backscattering or backreflection in a cross-sectional plane or volume.

Ultrasound imaging is a well established clinical imaging modality and is used in a wide range of applications ranging from imaging of internal organ systems, transluminal endoscopic imaging, and catheter-based intravascular imaging. In ultrasound, a high-frequency sound wave is launched into the material or tissue being imaged using an ultrasonic probe transducer [43–47]. The sound wave travels into the material or tissue and is reflected or backscattered from internal structures having different acoustic properties. The frequency of the sound wave determines the image resolution in ultrasound, with higher frequencies yielding higher resolutions. However, attenuation of the sound wave also occurs with propagation and higher frequencies have reduced imaging depths. The time behavior or echo structure of the reflected sound waves is detected by the ultrasonic probe and the ranges and dimensions of internal structures determined from the echo delay. This principle is also similar to that used in radar range detection of aircraft.

In OCT, measurements of distance and microstructure are performed by backreflecting and backscattering light waves from different microstructural features within the material or tissue [1]. For the purposes of illustration, it is possible to visualize the operation of OCT by thinking of the light beam as being composed of short optical pulses. However, it is important to note that although OCT may be performed using short pulse light, most OCT systems operate using continuous-wave short coherence length light. In addition, a wide range of other OCT measurement approaches have been demonstrated which measure the spectral properties of low-coherence light or use rapidly tunable narrow linewidth light.

When a beam of sound or light is directed onto tissue, it is backreflected or backscattered from structures which have different acoustic or optical properties as well as from boundaries between structures. The dimensions of the different structures can be determined by measuring the "echo" time it takes for sound or light to be backreflected or backscattered from the different structures at varying axial (longitudinal) distances. In ultrasound, the axial measurement of distance or range is referred to as A mode scanning. The principal difference between ultrasound and optical imaging is the fact that the velocity of propagation of light is approximately a million times faster than the velocity of sound. Because distances within the material or tissue are determined by measuring the "echo" time delay of backreflected or backscattered light waves, this implies that distance measurement using light requires ultrafast time resolution.

Two of the most important parameters for characterizing imaging performance are image resolution and imaging depth. The resolution of ultrasound imaging depends directly on the frequency or wavelength of the sound waves which are used [43–47]. For typical clinical ultrasound systems, sound wave frequencies are in the ten megahertz (10 MHz) regime and yield spatial resolutions as fine as 150 μm. Ultrasound imaging has the advantage that sound waves at this frequency are readily transmitted into most biologic tissues and therefore it is possible to obtain images of structures up to several tens of centimeters deep within the body. The sound frequency is an important parameter in ultrasound imaging because it is possible to optimize image resolution for a given application while trading off image-penetration depths. High frequency ultrasound has been developed and investigated extensively in laboratory applications as well as some clinical applications. Resolutions of 15 to 20 μm have been achieved with frequencies of 100 MHz and higher. However, high frequency ultrasound is

strongly attenuated in biologic tissues and attenuation increases approximately in proportion to the frequency. Thus, high frequency ultrasound imaging is limited to depths of only a few millimeters. It is also important to note that the transverse resolution of ultrasound is governed by the ability to focus sound waves and in general sound is more difficult to focus than light, so transverse resolutions for ultrasound are lower than for OCT. Current OCT imaging technologies have resolutions ranging from 1 to 15 μm. The inherently high resolution of OCT permits the imaging of features such as tissue architectural morphology as well as some cellular features. The principal disadvantage of optical imaging is that light is highly scattered by most biologic tissues. In most tissues other than the eye, optical scattering limits image penetration depths to 2 to 3 mm.

Finally it is helpful to point out that OCT, ultrasound, and microscopy have different mechanisms of contrast in images. Ultrasound images are differences in mismatch of acoustic impedance of ultrasound scattering between different tissues. This generates differences in the intensity of reflected or backscattered sound waves. OCT imaging uses light and is sensitive to differences in index of refraction of optical scattering between different tissues. Finally, in microscopy, images are generated by differences in either optical reflection or transmission through thin sections. In histopathology, a wide variety of stains can be used to selectively enhance contrast between different structures. Thus, the appearance of OCT images is, in general, different from either ultrasound or histopathology and studies are required to establish a basis for interpreting OCT images in terms of clinically relevant pathology.

Principles of Operation and Technology of Optical Coherence Tomography

Because the velocity of light is extremely high, its echo time delay cannot be measured directly by electronics as in ultrasound. The velocity of sound in water is approximately 1500 m/sec, whereas the velocity of light is approximately 3×10^8 m/sec. Distance or spatial information may be determined from the time delay of reflected echoes according to the formula $\Delta T = z/v$ where ΔT is the echo delay, z is the distance that the echo travels, and v is the velocity of the sound wave or light wave. The measurement of distances or dimensions with a resolution on the 100-micron scale, which would be typical for ultrasound, corresponds to a time resolution of approximately 100 nsec (100×10^{-9} sec). The echo time delays associated with light are extremely rapid. For example, the measurement of a structure with a resolution on the 10-micron scale, which is typical in OCT, corresponds to a time resolution of approximately 30 fsec (30×10^{-15} sec). Direct electronic detection is not possible on this time scale. Instead, it is necessary to use correlation or interferometry techniques. One method for measuring the echo time delay of light is to use low-coherence interferometry. Low-coherence interferometry was first developed for measuring reflections in fiber optics and optoelectronic devices [48–50]. The first applications of low-coherence interferometry in biomedicine were in ophthalmology to perform precision measurements of axial eye length and corneal thickness [51,52].

Low-coherence interferometry measures the echo time delay and intensity of backscattered light by comparing it to light that has traveled a known reference path length and time delay. Measurements are performed using a Michelson type interferometer (Figure 1). Light from a source is directed onto a beam splitter and one of the beams is incident onto the sample to be imaged, while the second beam travels a reference path with a variable path length and time delay. The backscattered light from the sample is interfered with reflected light from the reference arm and detected with a photodetector at the output of the interferometer. If the light source is coherent, then interference fringes will be observed as the relative path lengths are varied. However, if low-coherence or short pulse light is used, then interference of the light reflected from the sample and reference path can occur only when the two path lengths match to within the coherence length of the light. The echo time delay and intensity of backscattered light from sites within the sample can be measured by detecting and demodulating the interference output of the interferometer while scanning the reference path length.

Figure 2 shows a schematic illustrating how OCT performs cross-sectional imaging. The optical beam is focused into the sample being imaged, and the echo time delay and intensity of the backscattered light are measured to yield an axial backscattering profile. The incident beam is then scanned in the transverse direction, and the axial backscattering profile is measured at several transverse positions to yield a two-dimensional data set. This data set

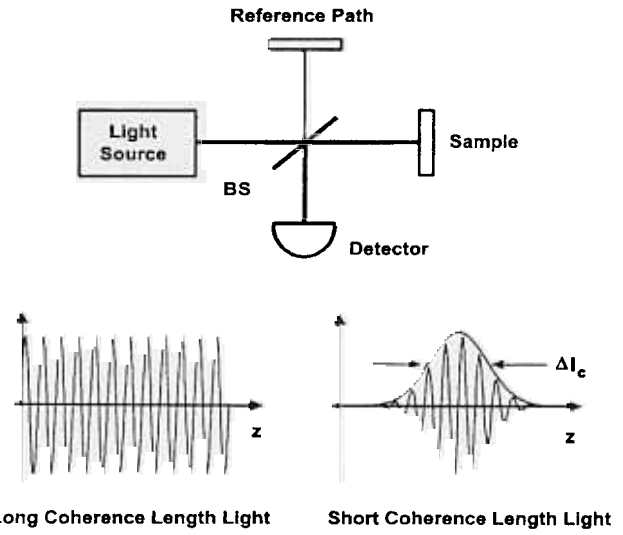

Figure 1. *OCT performs imaging by measuring the echo time delay of reflected light using low-coherence interferometry. The system is based on a Michelson type interferometer. Reflections or backscattering from the object being imaged are correlated with light which travels a reference path.*

represents the optical backscattering through a cross section of the tissue. The data is displayed as a logarithmic gray scale or false color image.

In contrast to conventional microscopy, the mechanisms which govern the axial and transverse image resolution in OCT are decoupled. The axial resolution in OCT imaging is determined by the coherence length of the light source so high resolution can be achieved independent of the beam focusing conditions. The interference signal detected at the output of the interferometer is the electric-field autocorrelation of the light source. The coherence length is the spatial width of this field autocorrelation. In addition, the envelope of the field autocorrelation is equivalent to the Fourier transform of the power spectrum. Thus, the width of the autocorrelation function, or the axial resolution, is inversely proportional to the width of the power spectrum. For a source with a Gaussian spectral distribution, the axial resolution Δz is:

$$\Delta z = (2 \ln 2/\pi)(\lambda^2/\Delta\lambda)$$

where Δz and $\Delta\lambda$ are the full widths at half maximum of the autocorrelation function and power spectrum respectively and λ is the source center wavelength. The axial resolution is inversely proportional to the bandwidth of the light source, and thus high resolution may be achieved by using broad bandwidth optical sources.

The transverse resolution achieved with an OCT imaging system is determined by the focused spot size as in conventional microscopy. The transverse resolution is:

$$\Delta x = (4\lambda/\pi)(f/d)$$

where d is the spot size on the objective lens and f is its focal length. High transverse resolution can be obtained by using a large numerical aperture and focusing the beam to a small spot size. In addition, the transverse resolution is also related to the depth of focus or the confocal parameter b:

$$b = \pi\Delta x^2/2\lambda$$

Increasing the transverse resolution (smaller Δx) produces a decrease in the depth of focus, as in conventional microscopy.

Finally, the signal-to-noise of detection can be calculated using standard techniques from optical communications theory and is given by:

$$SNR = 10Log(\eta P/2h\nu NEB)$$

where P is the detected power, NEB is the noise equivalent bandwidth of the detection, η is the detector quantum efficiency, and $h\nu$ is the photon energy. The signal-to-noise ratio scales with the reflected or backscattered power divided by the noise equivalent bandwidth of the detection. This means that higher image acquisition speeds or higher image

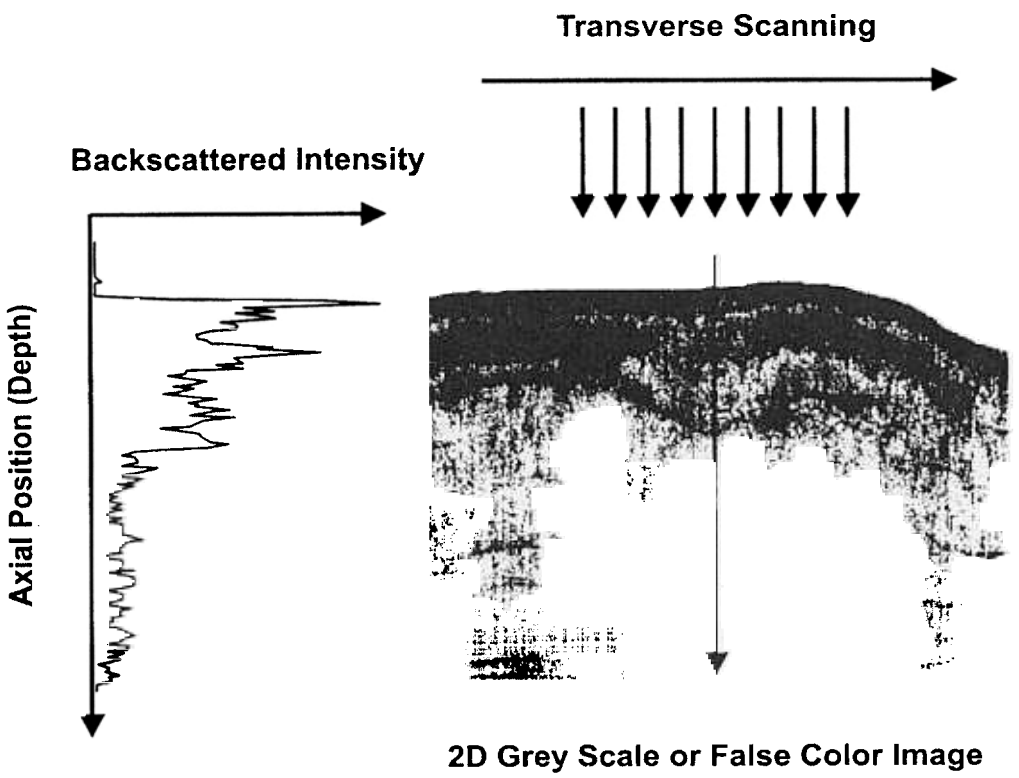

Figure 2. *Cross-sectional images are constructed by performing measurements of the echo time delay of light at different transverse positions. The result is a two-dimensional data set which represents the backscattering in a cross-sectional plane of the tissue. This data can be displayed as a gray scale or false color image.*

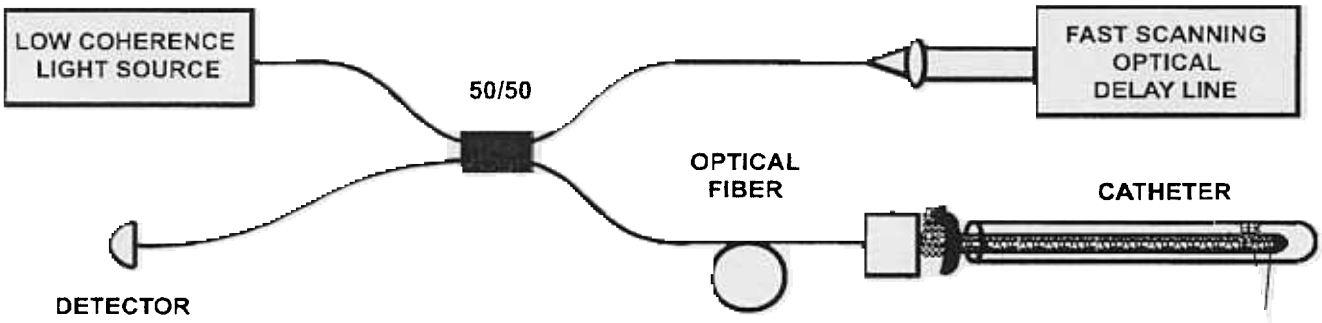

Figure 3. *Schematic of OCT instrument based on a fiber optic implementation of a Michaelson interferometer. One arm of the interferometer is interfaced to the measurement instrument and the other arm has a scanning delay line. The system shown is configured for high-speed catheter/endoscope-based imaging. The technology can be engineered into a compact and clinically viable form.*

resolutions require higher optical powers for a given signal-to-noise ratio.

One of the advantages of OCT is that it can be implemented using compact fiber optic components and integrated with a wide range of medical instruments. Figure 3 shows a schematic of an OCT system using a fiber optic Michelson type interferometer. A low-coherence light source is coupled into the interferometer and the interference at the output is detected with a photodiode. One arm of the interferometer emits a beam which is directed and scanned on the sample which is being imaged, whereas the other arm of the interferometer is a reference arm with a scanning delay line.

For research applications, short pulse lasers are used as light sources for OCT imaging because they have extremely short coherence lengths and high output powers, enabling high-resolution, high-speed imaging. Many of our studies were performed using a short pulse Cr^{4+}: Forsterite laser. This laser produces output powers of 100 mW generating ultrashort pulses at wavelengths near 1300 nm and can produce bandwidths sufficient to achieve an axial resolution of 5 to 10 μm [35]. Using incident powers in the 1 to 10 mW range, image acquisition speeds of several frames per second and signal-to-noise ratios of 100 dB are achieved. In other studies, a short pulse Ti:Al_2O_3 laser operating near 800 nm has been used to achieve axial resolutions as fine as 1 μm [36]. For clinical applications, compact superluminescent diodes or semiconductor-based light sources are more convenient than short pulse lasers. Commercially available (AFC Technologies, Hull, Quebec, Canada) sources operating at 1300 nm can achieve axial resolutions of $\sim$15 μm with output powers of 10 to 15 mW, sufficient for real-time OCT imaging.

Biomedical Imaging Using Optical Coherence Tomography

Several features of OCT suggest that it will be an important technology for biomedical imaging.

1. OCT can image with axial resolutions of 1 to 15 μm, one to two orders of magnitude higher than conventional ultrasound. This resolution approaches that of histopathology, allowing architectural morphology and some cellular features to be resolved. Unlike ultrasound, imaging can be performed directly through air without requiring direct contact with the tissue or a transducing medium.

2. Imaging can be performed *in situ*, without the need to excise a specimen. This enables imaging of structures in which biopsy would be hazardous or impossible. It also allows better coverage, reducing the sampling errors associated with excisional biopsy.

3. Imaging can be performed in real time, without the need to process a specimen as in conventional biopsy and histopathology. This allows pathology to be monitored on screen and stored on high-resolution video tape. Real-time imaging can enable real-time diagnosis, and coupling this information with surgery, it can enable surgical guidance.

4. OCT is fiber optically based and can be interfaced to a wide range of instruments including catheters, endoscopes, laparoscopes, and surgical probes. This enables imaging of organ systems inside the body.

5. Finally, OCT is compact and portable, an important consideration for a clinically viable device.

Ophthalmic Imaging

OCT was initially applied for imaging of the eye [3–7]. To date, OCT has had the largest clinical impact in ophthalmology. Figure 4 shows an example of an OCT image of the normal retina of a human subject [5]. This image is 250 transverse pixels wide and imaging was performed using a wavelength of 800 nm with a 10-μm resolution. The OCT image provides a cross-sectional view of the retina with unprecedented high resolution and allows detailed structures to be differentiated. Although the retina is almost transparent and has extremely low optical backscattering, the high sensitivity of OCT imaging allows extremely weak backscattering features such as the vitreal-retinal junction to be visualized. The retinal pigment epithelium and choroid, which is highly vascular, are visible as highly scattering structures in the OCT image. The retinal nerve fiber layer is visible as a scattering layer originating from the optic disk and becoming thinner approaching the fovea. The total retinal thickness as

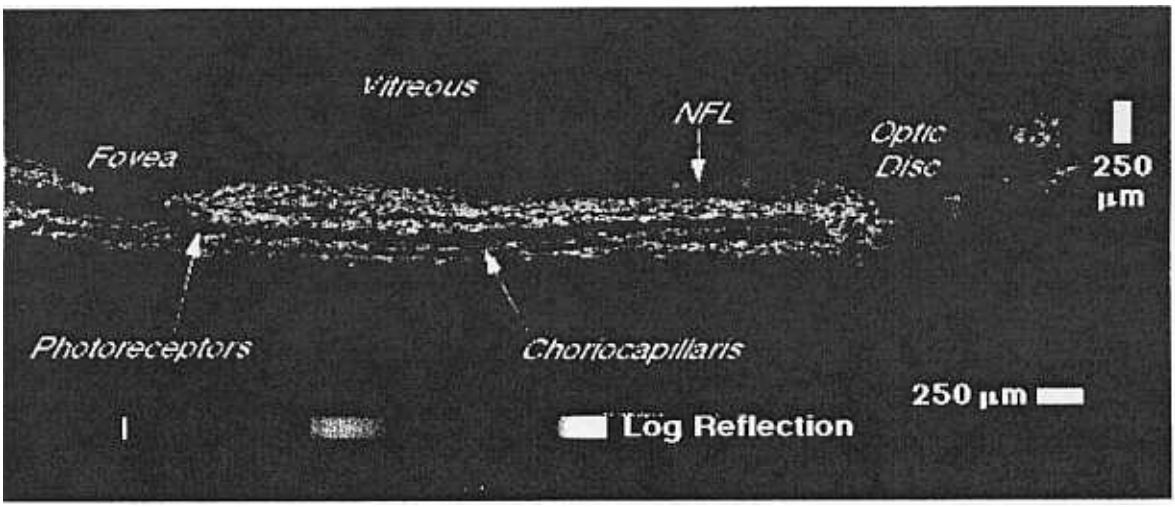

Figure 4. *OCT image of the human retina papillary-macular axis in vivo illustrating the ability to discriminate structural morphology. The optic disk as well as several of the retinal layers are observed. The highly backscattering retinal nerve fiber layer (NFL) and choriocapillaris appear red in the false color image. From Ref. [5].*

well as the retinal nerve fiber layer thickness can be measured. Because these images have a resolution of 10 μm, there can be residual motion of the patient's eye on the 1 to 2 second time scale necessary for the measurement. However, because OCT measures absolute position, image-processing algorithms can be used to measure the axial motion of the eye and correct for motion artifacts [3].

Clinical studies have been performed to investigate the feasibility of using OCT for the diagnosis and monitoring of retinal diseases such as glaucoma, macular edema, macular hole, central serous chorioretinopathy, age related macular degeneration, epiretinal membranes, optic disc pits, and choroidal tumors [5,53–59]. In addition, the ability of OCT to perform real-time imaging has also been used to study

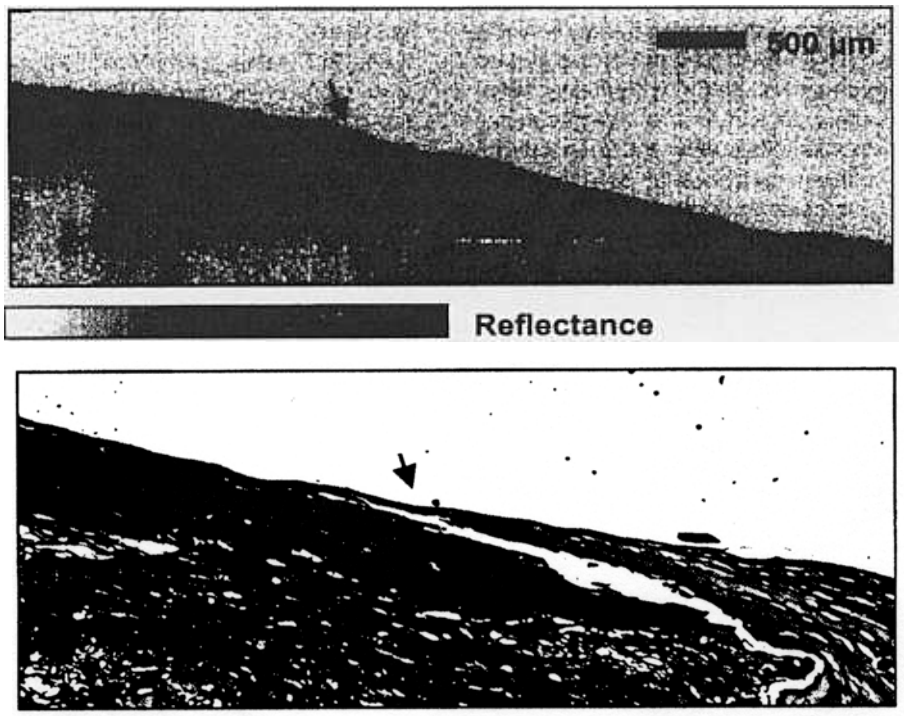

Figure 5. *OCT image of atherosclerotic plaque in vitro and corresponding histology. The plaque is heavily calcified with a low lipid content. A thick intimal layer covers the plaque. The high resolution of OCT can resolve small structures such as the thin intimal layer which are associated with unstable plaques. From Ref. [11].*

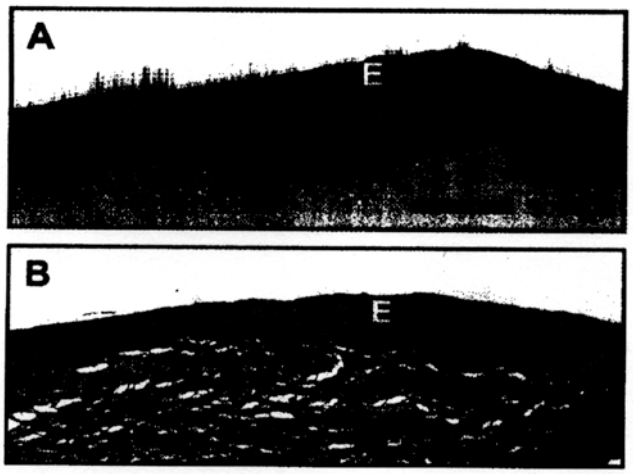

Figure 6. *OCT image of cervix imaged in vitro showing the ability to differentiate architectural morphology (image size: 1.5 mm × 2 mm, resolution: 6 μm × 10 μm). The epithelial layer (e) of the ectocervix and the basal membrane (arrow) were clearly identified. From Ref. [26].*

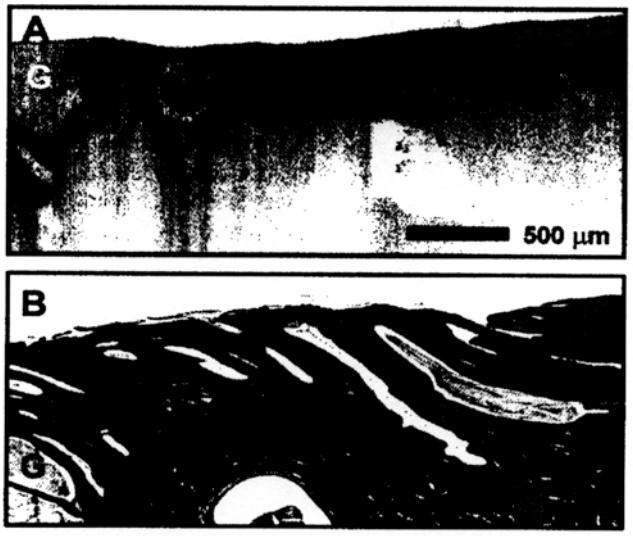

Figure 7. *OCT image of the ectocervix in vitro. Deep endocervical glands (g), some of which developed into fluid filled cysts, were also visible and are a finding common in postmenopausal women. From Ref. [26].*

dynamic responses of the retina including retinal laser injury [60]. Images can be analyzed quantitatively and processed using intelligent algorithms to extract features such as retinal or retinal nerve fiber layer thickness [61–64]. Mapping and display techniques have been developed to represent the tomographic data in alternate forms, such as thickness maps, to aid interpretation. OCT is especially promising for the diagnosis and monitoring of diseases such as glaucoma or macular edema associated with diabetic retinopathy because it can provide quantitative information retinal pathology which is a measure of disease progression. OCT

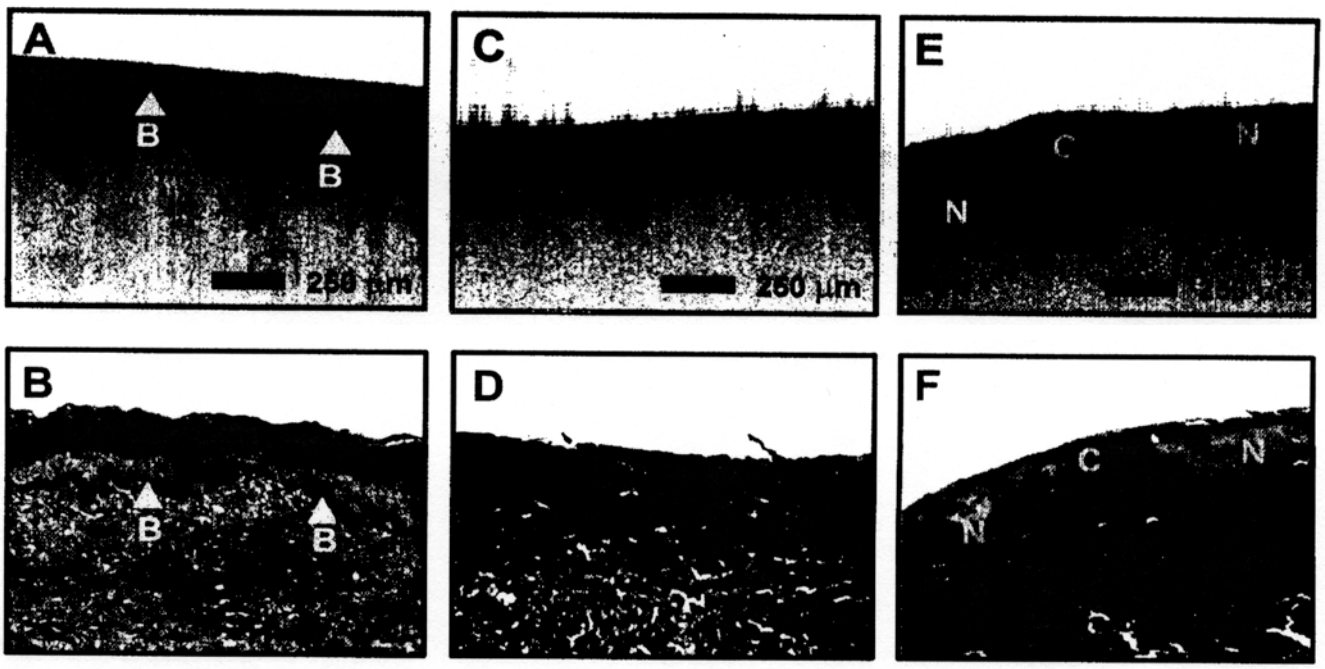

Figure 8. *Cervical disease imaged in vitro (image size: 3 mm×2 mm, resolution: 6 μm × 10 μm). (A) Carcinoma in situ is characterized by a thick, irregular epithelial layer in addition to thickening of the basement membrane (B). (C and E) Images of invasive carcinoma show a heterogeneous surface with the basement membrane no longer defined. Distinct backscattering patterns can be noted in cellular (C) and noncellular (N) regions. Images are correlated with histopathology. From Ref. [26].*

has the potential to detect and diagnose early stages of disease before physical symptoms and irreversible loss of vision occur.

Imaging In Nontransparent Tissues

With recent research advances, OCT imaging of optically scattering, nontransparent tissues has become possible, thus enabling a wide variety of biomedical applications [8–11]. One of the most important advances for imaging in optically scattering tissues was the use of longer wavelengths where optical scattering is reduced. By performing OCT imaging at 1300-nm wavelengths, image penetration depth of 2 to 3 mm can be achieved in most tissues. This imaging depth is comparable to the depth over which many biopsies are performed. In addition, many diagnostically important changes of tissue morphology occur at the epithelial surfaces of organ lumens.

One class of applications where OCT could be especially powerful is where conventional excisional biopsy is hazardous or impossible. For example, in ophthalmology, biopsy of the retina is impossible and OCT can provide high-resolution images of pathology that cannot be obtained using any other technique. Another scenario where biopsy is not possible is imaging of atherosclerotic plaque morphology in the coronary arteries [11,12]. Research has demonstrated that most myocardial infarctions result from the rupture of small to moderately sized cholesterol-laden coronary artery plaques followed by thrombosis and vessel occlusion [65–68]. The plaques at highest risk for rupture are those which have a structurally weak fibrous cap [69]. These plaque morphologies are difficult to detect by conventional radiologic techniques and their microstructural features cannot be determined. Identifying high-risk unstable plaques and patients at risk for myocardial infarction is important because of the high percentage of occlusions which result in sudden death [70]. OCT could be powerful for diagnostic intravascular imaging in both risk stratification and guidance of interventional procedures such as atherectomy.

In vitro imaging studies of arterial lesions were performed to investigate the correlation of OCT and histology [11]. Figure 5 shows an example of an unstable plaque morphology from a human abdominal aorta specimen and corresponding histology. Specimens were obtained after autopsy and were imaged by OCT using a microscope delivery system before fixation. OCT imaging was performed at 1300-nm wavelength using a superluminescent diode light source with axial resolutions of ~16 μm. The OCT image and histology show a small intimal layer covering a large atherosclerotic plaque which is heavily calcified and has a relatively low lipid content. The optical scattering properties of lipid, adiopse tissue, and calcified plaque are different and provide contrast between different structures and plaque morphologies. Currently, these lesions can only be accurately diagnosed by postmortem histology, and therefore interventional techniques cannot be used effectively to treat them. The ability to identify structural details such as the presence and thickness of intimal caps using catheter-based OCT imaging techniques could lead to significant improvements in patient risk stratification.

The rupture of unstable lipid-filled atherosclerotic plaques in coronary arteries is now believed to be the most common cause of acute myocardial infarction [65,67]. Conventional clinical imaging modalities such as angiography, ultrasound, or MRI do not have sufficient resolution to identify these lesions or to guide the removal of plaque through catheter-based atherectomy procedures. High-frequency (20 to 30 MHz) intravascular ultrasound or IVUS can be used to determine the extent of arterial stenosis and to guide intervention procedures such as stent deployment [71,72]. However, the resolution of IVUS is limited to approximately 100 μm, and thus it is difficult to decisively identify high-risk plaque morphologies [73]. Studies have been performed which compare IVUS and OCT imaging *in vitro* and demonstrate the ability of OCT to identify clinically relevant pathology [12]. *In vivo* OCT arterial imaging has also been performed in New Zealand White rabbits using a catheter-based delivery system [40]. Optical scattering from blood limits OCT imaging penetration depths so that saline flushing at low rates was required for imaging. These effects depend on vessel diameter as well as other factors and additional investigation is required.

Optical Biopsy and Detecting Early Neoplastic Changes

Identification of early neoplastic changes is important clinically because once metastatic, treatment is difficult. The diagnostic indicators of early neoplastic changes include accelerated rate of growth, mass growth, local invasion, lack of differentiation, anaplasia and metastasis. The evaluation of structural and cellular features of these types is necessary for the correct identification and grading of neoplasias. Changes in architectural morphology and glandular organization are relatively easy to identify because they fall within the resolution limits of most standard resolution OCT systems. As OCT technology improves, the ability to image cellular level features should improve, and the range of applicability of OCT imaging should increase.

In the following section we consider some examples of neoplasias in different tissues and organ systems which show the imaging capabilities of OCT. Most studies to date have focused on *in vitro* imaging and correlation with histopathology. *In vitro* studies have been performed to investigate OCT imaging in the gastrointestinal, urinary, respiratory, and female reproductive tracts [13–16,18,21–23,25–28]. Limited *in vivo* imaging studies in animals and human subjects have also been reported [15,28,41,42]. However, clinical feasibility studies in human subjects are just beginning, and clinical data should become available shortly.

Figures 6 and 7 shows examples of OCT images and corresponding histology of normal ectocervix and endocervix *in vitro*. Imaging studies of other gynecological neoplasias including endometrial and ovarian adenocarcinoma have also been reported [25]. Imaging was performed on fresh surgical and autopsy specimens before fixation. These

images were performed with a resolution of 6 μm axial by 10 μm transverse. After imaging, the specimens were fixed and processed for histology. Sections of 5-μm thickness were stained with hematoxylin and eosin. In the OCT image of Figure 7, the epithelial layer of the ectocervix and the basal membrane are clearly visible. Deep endocervical glands, some of which developed into fluid-filled cysts, were also visible and are a finding common in postmenopausal women. Figure 8 shows OCT images and corresponding histology of cervical specimens exhibiting carcinoma *in situ* and poorly differentiated carcinoma. In (Figure 8*A*), the carcinoma *in situ* is characterized by a thick, irregular epithelial layer in addition to thickening of the basement membrane. With invasive carcinoma (Figure 8, *C* and *E*), the tissue surface appears heterogeneous and the basement membrane is no longer defined.

These studies suggest that OCT imaging can differentiate changes in epithelial thickness, the integrity of the basement membrane, and glandular structure such as cysts. However, preliminary OCT imaging studies have not yet demonstrated the ability to differentiate subcellular morphologic changes. Thus, the ability to diagnose and grade dysplastic changes such as cervical intraepithelial neoplasia (CIN) remains an open question. In the United States, cervical cancer is not a major health problem due to the wide availability of cytologic screening techniques (Papanicolaou smear). However, cervical cancer remains a major health problem in many other countries. From the research viewpoint, the cervix is an excellent system for studies of OCT imaging because it exhibits a well-defined pathology and disease progression and imaging can be performed colposcopically with correlation to both colposcopic appearance and pathology. Preliminary clinical imaging studies of the cervix are currently underway and results should be reported shortly.

The gastrointestinal mucosae have well defined glandular organization which can be imaged with OCT [13,14,22,27]. Figure 9 shows an example of an OCT image of normal esophagus, normal colon, and ampullary carcinoma. The OCT image of the esophagus shows normal morphology of the mucosa and submucosa. The upper portion of the mucosa appears homogenous in the OCT image and is associated with squamous epithelial architecture. The muscularis mucosa is more highly reflective than the mucosa, and a gap can be seen between the muscularis mucosa and the submucosa. The OCT image of the colon shows normal glandular organization associated with columnar epithelial structure. The mucosa and muscularis mucosa can be differentiated due to the different backscattering characteristics within each layer. Architectural morphology such as crypts or glands within the mucosa can also be seen. Finally, the OCT image of ampullary carcinoma shows disruption of architectural morphology or glandular organization. The area on the right of the image is normal, whereas the carcinoma is on the left of the image. Hypertrophic and distorted crypts are characteristic of neoplastic changes in the bowel mucosa.

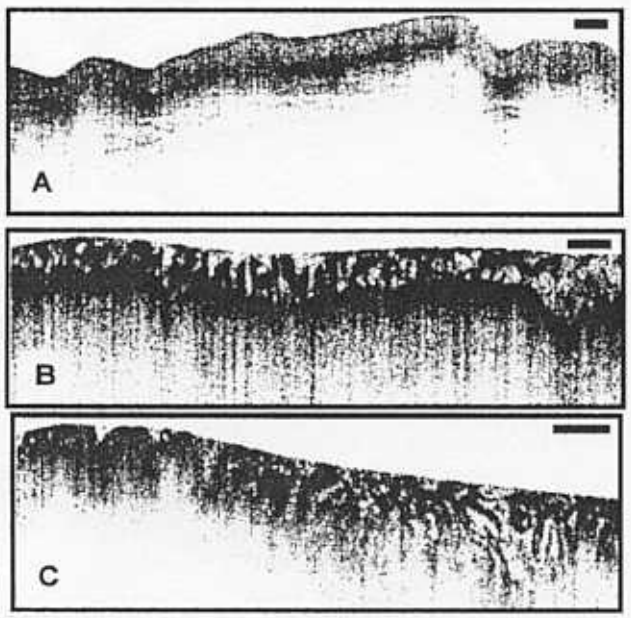

Figure 9. *OCT images of human gastrointestinal tissues and pathology in vitro showing the ability to differential epithelial structure and glandular organization. (A) normal human esophagus showing squamous epithelial structure, (B) normal colon with columnar epithelium and crypt structures, and (C) ampullary carcinoma showing associated disruption of normal epithelial organization. The carcinoma is evident on the left of the image. The bar is 500 μm. From Ref. [14].*

Catheter and Endoscopic OCT Imaging

To perform OCT imaging *in vivo*, it is necessary to develop image delivery systems for internal body imaging. Because OCT imaging technology is fiber-optic based, it can be easily integrated with many medical diagnostic instruments to enable internal body imaging. OCT laparascopes and hand-held surgical probes have recently been demonstrated [39]. Using fiber optics, a small-diameter transverse scanning catheter/endoscope has been developed [15,38]. The catheter/endoscope consists of a single-mode optical fiber encased in a hollow rotating torque cable. At the distal end of the catheter, the fiber is coupled to a graded index GRIN lens and a microprism to direct the OCT beam radially, perpendicular to the axis of the catheter. The rotating cable and distal optics are encased in a transparent housing. The OCT beam is scanned by rotating the cable to permit cross-sectional transluminal imaging, in a radar-like pattern, in vessels or hollow organs. Figure 10 shows a photograph of the prototype catheter. The catheter/endoscope has a diameter of 2.9 French or 1 mm, comparable to the size of a standard intravascular ultrasound catheter. This is small enough to allow imaging in a human coronary artery or insertion through the accessory port of a standard endoscope or bronchoscope.

The catheter/endoscope OCT system enables the acquisition of *in vivo* images of internal organ systems. *In vivo* imaging of the pulmonary, gastrointestinal, and urinary tracts as well as arterial imaging have been demonstrated in

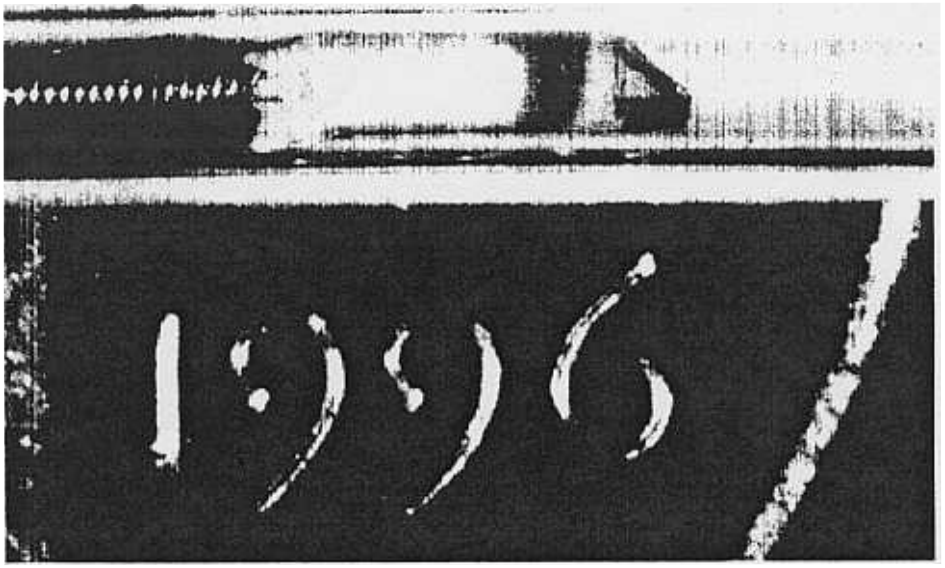

Figure 10. *Photograph of prototype OCT catheter for transverse, intraluminal imaging. The catheter consists of a single mode optical fiber contained in a rotating cable with a distal lens and prism. The rotating elements are housed in a stationary, transparent plastic sheath. The beam is emitted and scanned in a radial direction. The diameter of the catheter is 2.9 F or 1 mm.*

New Zealand White rabbits [15]. A short-pulse Cr^{4+}:forsterite laser was used as the light source for OCT system to achieve high-resolution with real-time image acquisition rates. The laser output wavelength was centered near 1280 nm with a full width at half maximum spectral bandwidth of 75 nm and 5 to 10 mW power was incident on the tissue. This yields an axial resolution of 10 μm and a signal-to-noise ratio of 110 decibels (dB). To achieve high-speed imaging at several frames per second, a novel high-speed scanning optical delay line was used in the OCT interferometer [33].

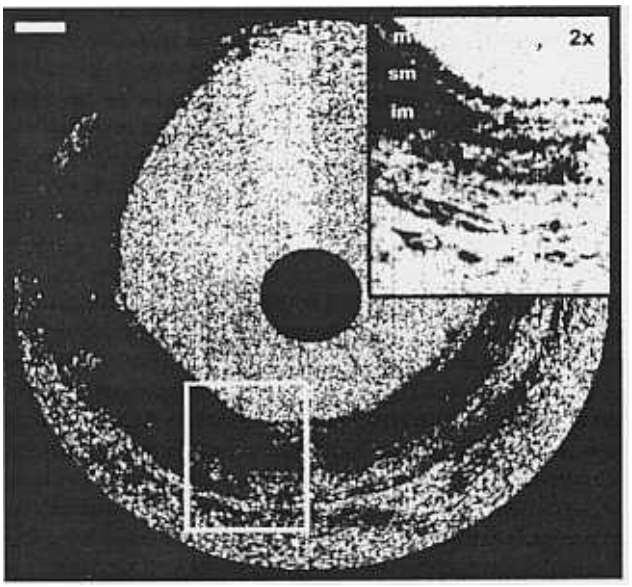

Figure 11. *OCT catheter/endoscope image in vivo of the esophagus of a New Zealand White Rabbit. The image is 512 pixels in circumference with 256 axial pixels and is acquired at four frames per second. The image clearly differentiates the layers of the esophagus including the mucosa, submucosa, inner muscularis, and outer muscularis. The bar is 500 μm. From Ref. [15].*

Figure 11 shows an example of *in vivo* OCT catheter/endoscope imaging of the rabbit gastrointestinal tract. The image shown was obtained with a 512 pixel lateral resolution at four frames per second to optimize lateral sampling. With recent advances in technology, two to four times higher image acquisition rates are possible. The two-dimensional image data were displayed using a polar coordinate transformation and inverse gray scale. Data were recorded in both Super VHS and digital format. As shown in Figure 11, OCT images of the esophagus *in vivo* permit excellent differentiation of mucosal morphology. The mucosa, submucosa, inner muscularis and outer muscularis can be visualized. The mucosa was readily identifiable because of its low optical backscattering compared with the submucosa. The ability to differentiate mucusal versus submucosal invasion can be an important criterion for determining therapy in early gastric and esophageal cancers.

Preliminary OCT imaging studies in patients have been reported [41,42]. More systematic OCT imaging studies comparing imaging with histologic or other diagnostic end-

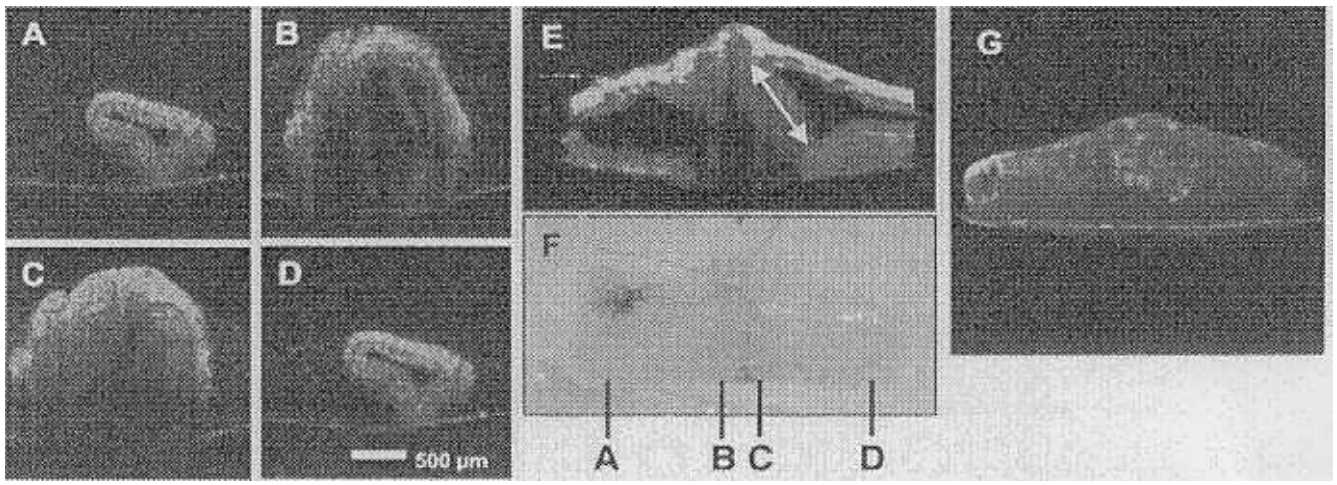

Figure 12. *OCT images of an anastomosis in a rabbit artery. The 1-mm-diameter rabbit artery was anastomosed with a continuous suture as seen in the digital image (F). Labeled lines in F indicate planes from which corresponding cross-sectional images were acquired. (A,D) Opposite ends of the anastomosis showing multilayered structure of the artery with a patent lumen. (B) Partially obstructed lumen and the presence of a thrombogenic flap. (C) Fully obstructed portion of the anastomosis site. Intraluminal features as seen in B and C are not observable from the en face microscope view. Three-dimensional projection shown in G can be arbitrary sectioned at any plane, such as the longitudinal section in E to show the obstruction. From Ref. [20].*

points are needed. Other research groups as well as our group are currently performing OCT imaging studies in patients, and results should be published shortly.

Comparison with Ultrasound

Endoscopic ultrasound has recently been introduced as a new technology for high-resolution endoscopic imaging [74–80]. Using ultrasound frequencies in the range of 10 to 30 MHz, axial resolutions in the range of 100 μm can be achieved [81–83]. Imaging of the esophagus or bowel requires filling the lumen with saline or using a liquid-filled balloon to couple the ultrasound into the tissue. Ultrasound can be used as an adjunct to endoscopy to diagnose and stage early esophageal and gastric neoplasms. Impressive results have been achieved using high frequency endoscopic ultrasound which demonstrate the differentiation of mucosal and submucosal structures.

Using OCT image resolutions of 15 μm or better can be achieved. This resolution enables the visualization of tissue architectural morphology. The imaging depth of OCT is 2 to 3 mm, less than that of ultrasound. However, many diseases

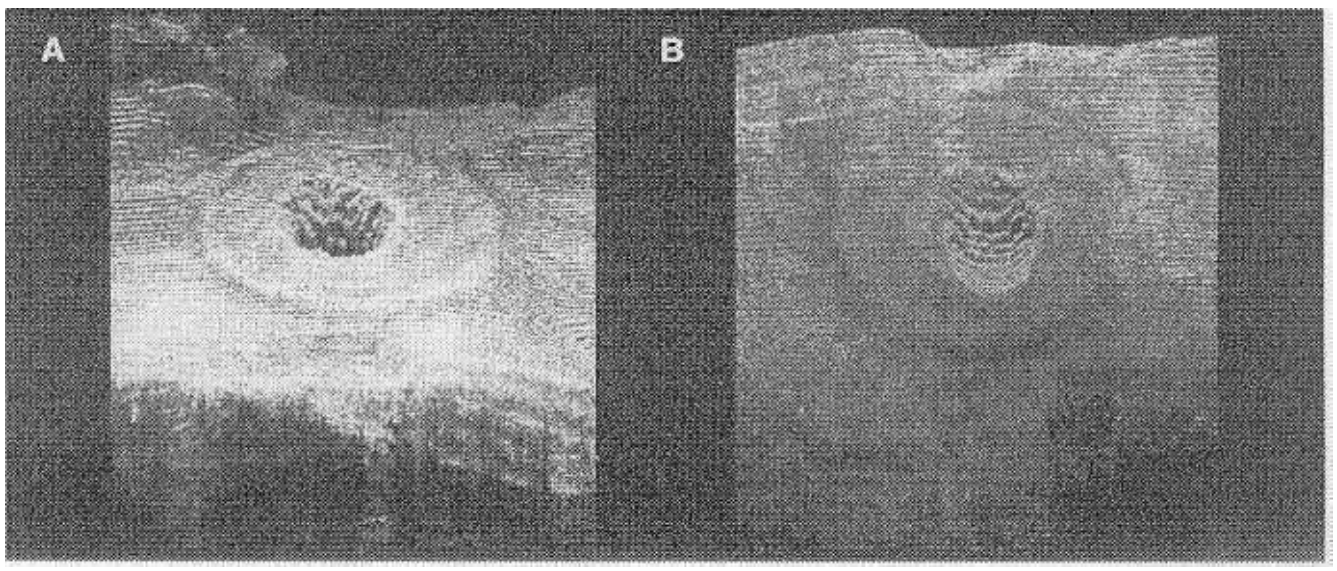

Figure 13. *Three-dimensional OCT projection image of a laser ablation crater. The lesion was produced by a 3-W, 10-s argon exposure of rat rectus abdominis muscle. The projection illustrates a central ablation crater and concentric zones of thermal injury. From Ref. [84].*

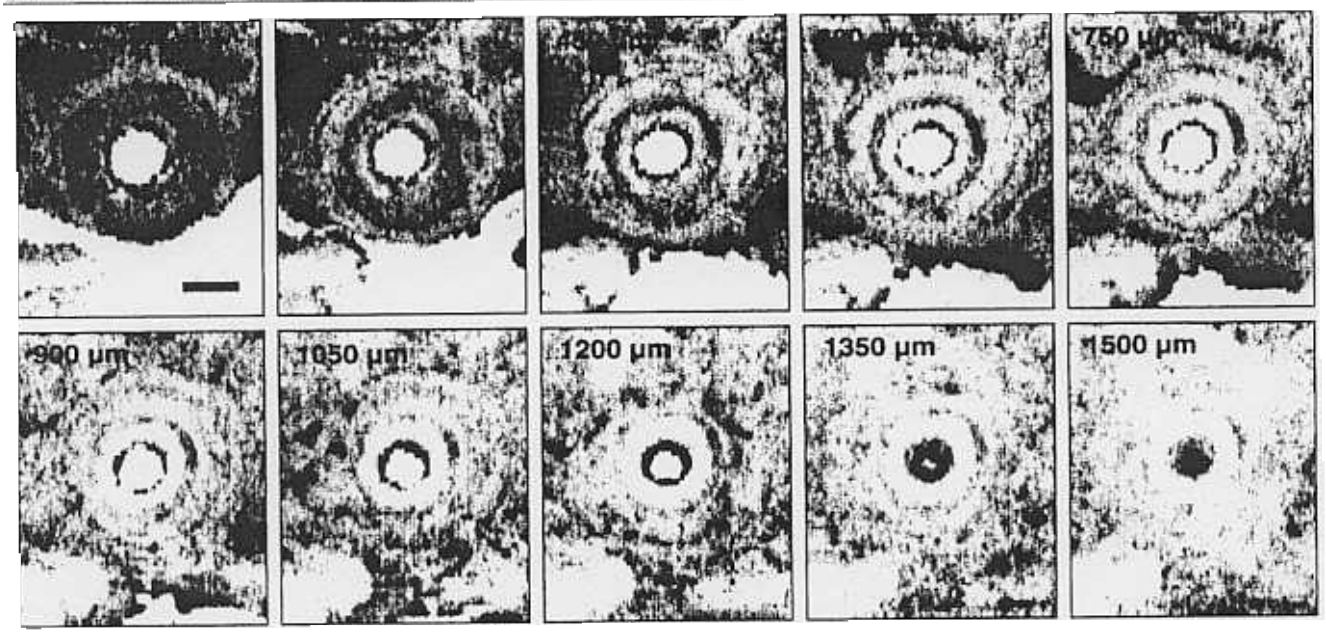

Figure 14. *En face images through ablation crater. En face sections in depth illustrate concentric zones of damage. Numbers refer to depth below surface. Bar represents 1 mm. From Ref. [84].*

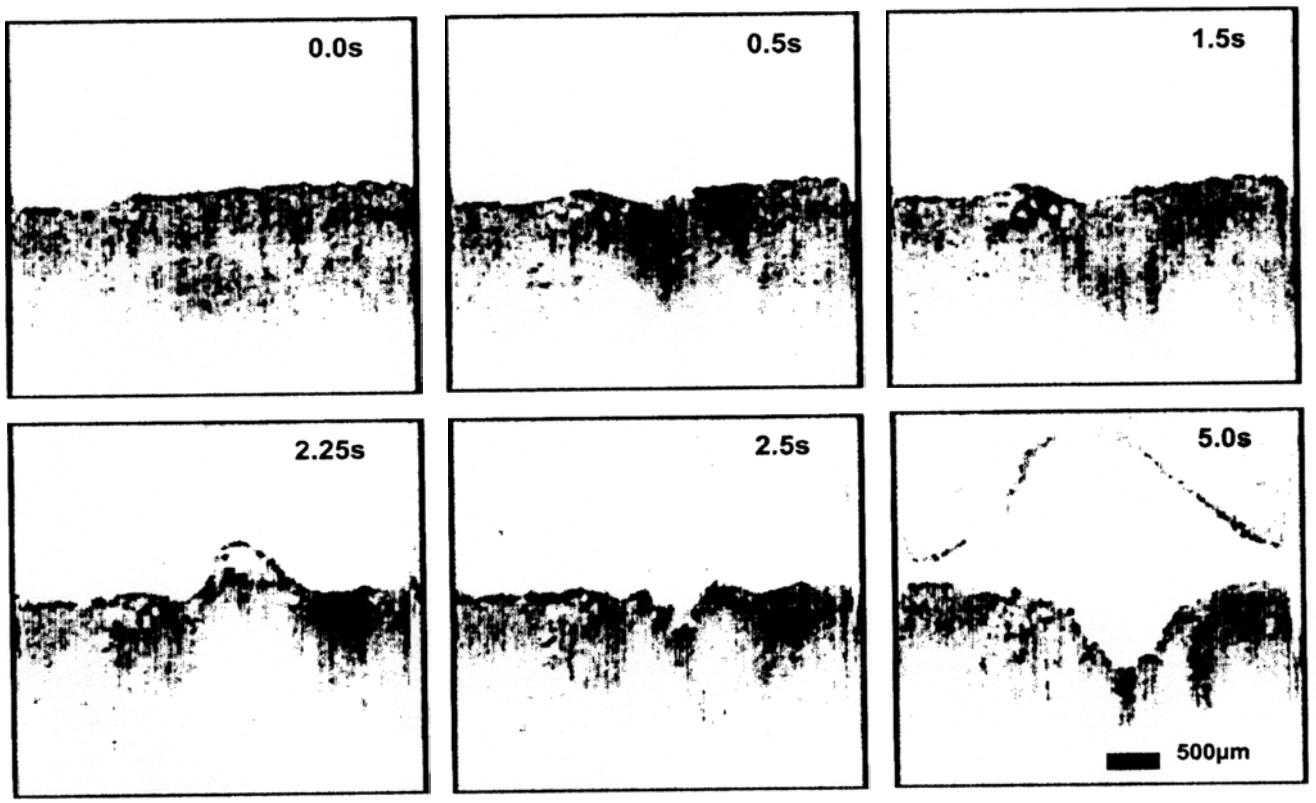

Figure 15. *Real-time imaging of ablation. Series of OCT images taken at eight frames per second during argon laser exposure of in vitro muscle (beef). Exposure parameters include 1-W laser power, 0.8-mm spot diameter on tissue. Times indicated are seconds post-exposure. At 2.25 seconds, the formation of a blister at the surface can be seen. The blister explodes (2.5 seconds) and a crater develops (5 seconds).*

originate from or involve the mucosa, submucosa, and muscular layers, and imaging the microscopic structure of small lesions or early neoplastic changes is well within the range of OCT.

Guiding Surgical Intervention

Another large class of applications for OCT is guiding surgical intervention. The ability to see beneath the surface of tissue in real time can guide surgery near sensitive structures such as vessels or nerves as well as assist in microsurgical procedures [17,19,20,26,27,84]. Optical instruments such as surgical microscopes are routinely used to magnify tissue to prevent iatrogenic injury and to guide delicate surgical techniques. OCT can be easily integrated with surgical microscopes. Hand-held OCT surgical probes and laparoscopes have also been demonstrated [39].

One example of a surgical application for OCT is the repair of small vessels and nerves following traumatic injury [85,86]. A technique capable of real-time, subsurface, three-dimensional, micron-scale imaging would permit the intraoperative monitoring of microsurgical procedures, giving immediate feedback to the surgeon which could improve outcome and enable difficult procedures. To demonstrate the use of OCT imaging for diagnostically assessing microsurgical procedures *in vitro* studies were performed using a microscope-based OCT system [20].

Figure 12 shows OCT images of an arterial anastomosis of a rabbit inguinal artery demonstrating the ability of OCT to assess internal structure and luminal patency. An artery segment was bisected cross-sectionally with a scalpel and then re-anastomosed using a No. 10-0 nylon suture with a 50-μm-diameter needle in a continuous suture. For precise registration of three-dimensional images, the anastomosed specimen was positioned on a micron step size, computer-controlled, motorized translation stage in the OCT microscope. A series of 40 cross-sectional images was acquired perpendicular to the long axis at 100-μm spacing. The specimen was also digitally imaged with a CCD camera. Cross-sectional OCT images (2.2×2.2 mm, 250×600 pixel) and three-dimensional projections of a 1-mm-diameter rabbit inguinal artery are shown. Figure 12, *A – D*, were acquired transversely at different positions through the anastomosis. The images of the ends of the artery clearly show arterial morphology corresponding to the intimal, medial, and adventitial layers of the elastic artery. The image from the site of the anastomosis shows that the lumen was obstructed by a tissue flap. By assembling a series of cross-sectional two-dimensional images, a three-dimensional data set was produced. Arbitrary planes can be selected and corresponding sections displayed. A three-dimensional projection of the arterial anastomosis is shown in Figure 12. The three-dimensional views can show microstructural features which are not evident in single cross-sectional images.

Because OCT can provide image information in real time, it can be integrated directly with surgery. In a recent study, we investigated the feasibility of using high-speed OCT imaging to guide the placement and image the dynamics of surgical laser ablation [84]. Argon laser ablation was performed in five different *ex vivo* rat organs to assess OCT imaging performance and variations between tissue types. The use of OCT to monitor ablative therapy in real-time could enable more precise control of laser delivery and reduction in iatrogenic injury. These studies were performed using a commercially available low-coherence light source (AFC Technologies, Hull, Quebec, Canada) having a center wavelength of 1310 nm and a free space axial resolution of 18 μm. The signal-to-noise ratio was 115 dB using 5 mW of incident power on the specimen. For typical tissues, this sensitivity permits imaging to depths up to 3 mm. For high-speed image acquisition, the size of the region imaged was 3×3 mm and 256×256 pixels. Images were displayed on a computer monitor and simultaneously recorded to Super VHS video tape. The acquisition rate was eight frames per second or 125 ms for each image.

The argon beam was aligned and centered within the OCT imaging plane. Specimens were obtained from Sprague-Dawley rats after euthanasia including brain, liver, kidney, lung, and rectus abdominis muscle. A three-dimensional micron-precision computer-controlled stage was used to position the specimen under the OCT imaging beam and was used to acquire three-dimensional data sets. Figure 13 shows a three-dimensional projection of a laser ablation crater in a rat rectus abdominis muscle. The laser exposure was 3 W of argon laser power focused to a 0.8-mm-diameter spot for 10 seconds. The OCT images show the ablation zone viewed from an external and an internal virtual viewpoint. Because image data is acquired over a three-dimensional volume, arbitrary cross-sectional tomographic planes can be synthesized. Figure 14 shows a series of *en face* images constructed at various depths through the ablation crater.

OCT imaging can also be performed of laser ablation in real time. Figure 15 shows an example of real-time OCT imaging during laser ablation of a bovine muscle specimen. The laser exposure was 2 W from the argon laser. At 0.5 seconds, changes in optical properties of the tissue are observed due to heating; explosive ablation begins at 2.25 s. These examples demonstrate the ability of OCT to perform real-time imaging as well as the use of image processing and rendering techniques to provide a more comprehensive view of tissue microstructure. OCT should improve intraoperative diagnostics by providing high-resolution, subsurface, cross-sectional imaging of vessels and nerves in real-time. Three dimensional imaging permits the assessment of the spatial orientation of morphology.

Cellular Level OCT Imaging

The development of high-resolution OCT is also an important area of active research. Increasing resolutions to the cellular and subcellular level are important for the diagnosis of early neoplasias as wall as other applications. As discussed previously, the axial resolution of OCT is determined by the coherence length of the light source used for imaging. Light sources for OCT imaging should have a

short coherence length or broad bandwidth, but also must have a single spatial mode so that they can be used in conjunction with interferometry. In addition, because the signal to noise depends on the incident power, light sources with average powers of several milliwatts are typically necessary to achieve real-time imaging. One approach for achieving high resolution is to use short pulse femtosecond solid state lasers as light sources [34,35,37].

High-resolution OCT imaging has been demonstrated *in vivo* in developmental biology specimens [36,37]. Figure 16 shows an example of high-resolution OCT images of a *X. laevis* (African frog) tadpole. The low-coherence light source used for imaging was a short pulse Ti:Al_2O_3 laser which generates pulse durations of ~5 fsec, corresponding to ~2 optical cycles. The laser operates near 800 nm and has a bandwidth of ~300 nm. Axial resolutions of 1.5 μm in free space or ~1 μm in the specimen have been achieved. The transverse resolution is 3 μm as measured by the focused spot size of the beam, whereas the axial resolution is measured by the width of the axial point spread function of a single reflection [36]. High transverse resolutions result in a decreased depth of field. However, the depth of field limitations can be overcome by using a technique similar to C mode scanning in ultrasound. A series of images can be acquired with different focus positions and fused into a single image with an enhanced zone of focus.

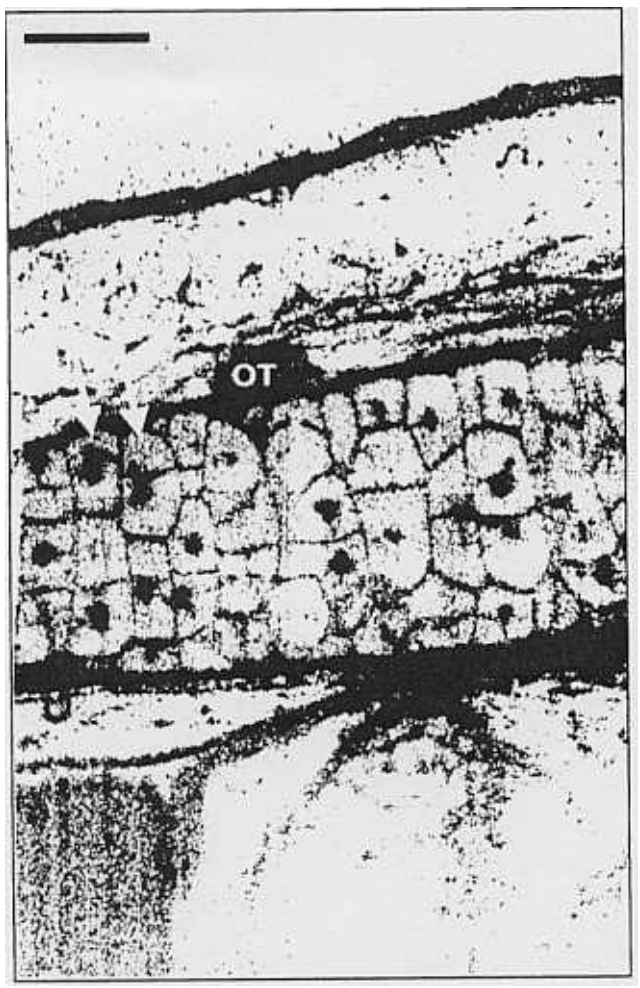

Figure 16. *Ultrahigh-resolution OCT images of a X. laevis (African frog) tadpole in vivo. The resolution is 1 μm axial by 3 μm transverse. The image is constructed by fusing multiple images with different focal positions (in analogy with C mode ultrasound) to overcome depth of field limitations associated with the fine transverse resolution. Cell membranes and individual cell nuclei are visible. From Ref. [36].*

Figure 16 shows the presence of multiple nuclei and cell membranes. The seemingly wide cell membranes in the OCT images are actually composed of membranes and extracellular matrix. The OCT image shows cells with varying size and nuclear-to-cytoplasmic ratios as well as cells undergoing mitosis. In developmental biology, the ability to image cellular and subcellular structure can be used to study mitotic activity and cell migration which occur during development. The extension of these results to human cells has important implications, but is challenging because differentiated human cells are smaller than developing cells. Additional improvements in resolution and technology are necessary to achieve this objective. In ophthalmology, improving resolution should allow more precise morphometric measurements of retinal features such as retinal thickness and retinal nerve fiber layer thickness, which are relevant for the detection and screening for macular edema and glaucoma. High-resolution imaging should also improve OCT diagnosis of early neoplastic changes. Standard OCT image resolutions are sufficient to image architectural morphology on the 10 to 15 μm scale and can identify many types of early neoplastic changes. However, the ability to image with cellular level resolution should not only enhance the spectrum of pathology that can be imaged, but also improve sensitivity and specificity. Current light sources for ultrahigh-resolution OCT imaging are based on short pulse lasers and are not clinically viable because of their complexity and expense. However, with the development of new technologies, especially in the telecommunications industry, compact and lower cost light sources should become available in the near future.

Discussion

It is unlikely that OCT can replace excisional biopsy and histology. However, from the viewpoint of screening and diagnosis of neoplasia, we expect that OCT may be used to guide standard excisional biopsy to reduce sampling errors and false negative results. This could improve the accuracy of biopsy as well as reduce the number of biopsies that are taken, resulting in cost savings. After more extensive clinical studies have been performed, it may be ultimately possible to use OCT to directly diagnose or grade early neoplastic changes in certain situations. This application will be more challenging because it implies making a diagnosis on the basis of OCT rather than conventional pathology and will only be possible in limited clinical situations. If these applications are successful, it would enable OCT diagnostic information to be immediately coupled to treatment decisions

and it may be possible to find scenarios where OCT can be used for real-time surgical guidance. The integration of diagnosis and treatment could improve outcome and by reducing the number of patient visits, yield a reduction in health care costs.

Each of these application scenarios requires a different level of performance in the ability to image tissue pathology. More importantly, it is necessary to demonstrate a sufficient level of sensitivity and specificity in clinical trials for a given clinical situation. Generally speaking, current OCT technology can be used to resolve morphologic features on several dimension scales ranging from architectural morphology or glandular organization (10 to 15 μm). As OCT technology improves, resolutions are approaching the cellular level (1 to 10 μm). Tissue contrast, the ability to differentiate morphology, and image quality are highly dependent on the specific structures being imaging. Because cancer is a highly heterogeneous disease, characterized by a spectrum of morphologic changes, etiologies, etc., we expect that the viability of OCT will be highly dependent on the details of the specific clinical application.

Summary

OCT can perform a type of optical biopsy, the micron-scale imaging of tissue morphology *in situ* and in real time. Image information is available immediately without the need for excision and histologic processing of a specimen. The development of high-resolution and high-speed OCT technology as well as OCT compatible catheter/endoscopes and other delivery systems represent enabling steps for many future OCT imaging clinical applications. More research remains to be done and numerous clinical studies must be performed to determine in which clinical situations OCT can play a role. However, the unique capabilities of OCT imaging suggest that it has the potential to have a significant impact on the diagnosis and clinical management of many diseases.

Acknowledgements

The scientific contributions of Xingde Li, Wolfgang Drexler, Joel Schuman, Annekathryn Goodman, Michael Hee, Brett Bouma, Gary Tearney, and Juergen Herrmann and Christine Jesser are gratefully acknowledged.

References

[1] Huang D, Swanson EA, Lin CP, Schuman JS, Stinson WG, Chang W, Hee MR, Flotte T, Gregory K, Puliafito CA, and Fujimoto JG (1991). Optical coherence tomography. *Science* **254**, 1178–1181.

[2] Fercher AF, Hitzenberger CK, Drexler W, Kamp G, and Sattmann H (1993). *In vivo* optical coherence tomography. *Am J Ophthalmol* **116**, 113–114.

[3] Swanson EA, Izatt JA, Hee MR, Huang D, Lin CP, Schuman JS, Puliafito CA, and Fujimoto JG (1993). *In vivo* retinal imaging by optical coherence tomography. *Opt Lett* **18**, 1864–1866.

[4] Izatt JA, Hee MR, Swanson EA, Lin CP, Huang D, Schuman JS, Puliafito CA, and Fujimoto JG (1994). Micrometer-scale resolution imaging of the anterior eye *in vivo* with optical coherence tomography. *Arch Ophthalmol* **112**, 1584–1589.

[5] Hee MR, Izatt JA, Swanson EA, Huang D, Schuman JS, Lin CP, Puliafito CA, and Fujimoto JG (1995). Optical coherence tomography of the human retina. *Arch Ophthalmol* **113**, 325–332.

[6] Puliafito CA, Hee MR, Lin CP, Reichel E, Schuman JS, Duker JS, Izatt JA, Swanson EA, and Fujimoto JG (1995). Imaging of macular diseases with optical coherence tomography. *Ophthalmology* **102**, 217–229.

[7] Puliafito CA, Hee MR, Schuman JS, and Fujimoto JG (1996). Optical Coherence Tomography of Ocular Diseases. Slack Inc, Thorofare, NJ.

[8] Schmitt JM, Knuttel A, Yadlowsky M, and Eckhaus MA (1994). Optical coherence tomography of a dense tissue — statistics of attenuation and backscattering. *Phys Med Biol* **39**, 1705–1720.

[9] Schmitt JM, Yadlowsky M, and Bonner RF (1995). Subsurface imaging of living skin with optical coherence tomography. *Dermatology* **191**, 93–98.

[10] Fujimoto JG, Brezinski ME, Tearney GJ, Boppart SA, Bouma B, Hee MR, Southern JF, and Swanson EA (1995). Optical biopsy and imaging using optical coherence tomography. *Nat Med* **1**, 970–972.

[11] Brezinski ME, Tearney GJ, Bouma BE, Izatt JA, Hee MR, Swanson EA, Southern JF, and Fujimoto JG (1996). Optical coherence tomography for optical biopsy: properties and demonstration of vascular pathology. *Circulation* **93**, 1206–1213.

[12] Brezinski ME, Tearney GJ, Weissman NJ, Boppart SA, Bouma BE, Hee MR, Weyman AE, Swanson EA, Southern JF, and Fujimoto JG (1997). Assessing atherosclerotic plaque morphology: Comparison of optical coherence tomography and high frequency intravascular ultrasound. *Br Heart J* **77**, 397–404.

[13] Izatt JA, Kulkarni MD, Hsing-Wen W, Kobayashi K, and Sivak MV, Jr (1996). Optical coherence tomography and microscopy in gastrointestinal tissues. *IEEE J Sel Top Quantum Electron* **2**, 1017–1028.

[14] Tearney GJ, Brezinski ME, Southern JF, Bouma BE, Boppart SA, and Fujimoto JG (1997). Optical biopsy in human gastrointestinal tissue using optical coherence tomography. *Am J Gastroenterol* **92**, 1800–1804.

[15] Tearney GJ, Brezinski ME, Bouma BE, Boppart SA, Pitris C, Southern JF, and Fujimoto JG (1997). *In vivo* endoscopic optical biopsy with optical coherence tomography. *Science* **276**, 2037–2039.

[16] Tearney GJ, Brezinski ME, Southern JF, Bouma BE, Boppart SA, and Fujimoto JG (1997). Optical biopsy in human urologic tissue using optical coherence tomography. *J Urol* **157**, 1915–1919.

[17] Brezinski ME, Tearney GJ, Boppart SA, Swanson EA, Southern JF, and Fujimoto JG (1997). Optical biopsy with optical coherence tomography, feasibility for surgical diagnostics. *J Surg Res* **71**, 32–40.

[18] Tearney GJ, Brezinski ME, Southern JF, Bouma BE, Boppart SA, and Fujimoto JG (1998). Optical biopsy in human pancreatobiliary tissue using optical coherence tomography. *Dig Dis Sci* **43**, 1193–1199.

[19] Boppart SA, Brezinski ME, Pitris C, and Fujimoto JG (1998). Optical coherence tomography for neurosurgical imaging of human intracortical melanoma. *Neurosurgery* **43**, 834–841.

[20] Boppart SA, Bouma BE, Pitris C, Southern JF, Brezinski ME, and Fujimoto JG (1998). Intraoperative assessment of microsurgery with three-dimensional optical coherence tomography. *Radiology* **208**, 81–86.

[21] Colston BW, Sathyam US, DaSilva LB, Everett MJ, Stroeve P, and Otis LL (1998). Dental OCT. *Opt Express* **3**, 230–238.

[22] Kobayashi K, Izatt JA, Kulkarni MD, Willis J, and Sivak MV (1998). High-resolution cross-sectional imaging of the gastrointestinal tract using optical coherence tomography: preliminary results. *Gastrointest Endosci* **47**, 515–523.

[23] Pitris C, Brezinski ME, Bouma BE, Tearney GJ, Southern JF, and Fujimoto JG (1998). High resolution imaging of the upper respiratory tract with optical coherence tomography — A feasibility study. *Am J Respir Crit Care Med* **157**, 1640–1644.

[24] Roper SN, Moores MD, Gelikonov GV, Feldchtein FI, Beach NM, King MA, Gelikonov VM, Sergeev AM, and Reitze DH (1998). *In vivo* detection of experimentally induced cortical dysgenesis in the adult rat neocortex using optical coherence tomography. *J Neurosci Methods* **80**, 91–98.

[25] Boppart SA, Goodman A, Libus J, Pitris C, Jesser C, Brezinski ME, and Fujimoto JG (1999). High resolution imaging of endometriosis and ovarian carcinoma with optical coherence tomography: feasibility for laparoscopic-based imaging. *Br J Obstet Gynaecol* **106**, 1071–1077.

[26] Pitris C, Goodman A, Boppart SA, Libus JJ, Fujimoto JG, and Brezinski ME (1999). High-resolution imaging of gynecologic neoplasms using optical coherence tomography. *Obstet Gynecol* **93**, 135–139.

[27] Pitris C, Jesser C, Boppart SA, Stamper D, Brezinski ME, and Fujimoto JG (1999). Feasibility of optical coherence tomography for high resolution imaging of human gastrointestinal tract malignancies. *J Gastroenterol*, in press.

[28] Jesser CA, Pitris C, Stamper DL, Boppart SA, Nielsen GP, Brezinski ME, and Fujimoto JG (1999). High resolution endoscopic evaluation of transitional cell carcinoma with optical coherence tomography. *Br J Radiol*, in press.

[29] Boppart SA, Brezinski ME, Bouma BE, Tearney GJ, and Fujimoto JG (1996). Investigation of developing embryonic morphology using optical coherence tomography. *Dev Biol* **177**, 54–63.

[30] Boppart SA, Bouma BE, Brezinski ME, Tearney GJ, and Fujimoto JG (1996). Imaging developing neural morphology using optical coherence tomography. *J Neurosci Methods* **70**, 65–72.

[31] Boppart SA, Tearney GJ, Bouma BE, Southern JF, Brezinski ME, and Fujimoto JG (1997). Noninvasive assessment of the developing *Xenopus* cardiovascular system using optical coherence tomography. *Proc Natl Acad Sci USA* **94**, 4256–4261.

[32] Tearney GJ, Bouma BE, Boppart SA, Golubovic B, Swanson EA, and Fujimoto JG (1996). Rapid acquisition of *in vivo* biological images by use of optical coherence tomography. *Opt Lett* **21**, 1408–1410.

[33] Tearney GJ, Bouma BE, and Fujimoto JG (1997). High-speed phase- and group-delay scanning with a grating-based phase control delay line. *Opt Lett* **22**, 1811–1813.

[34] Bouma B, Tearney GJ, Boppart SA, Hee MR, Brezinski ME, and Fujimoto JG (1995). High-resolution optical coherence tomographic imaging using a mode-locked Ti–Al_2O_3 laser source. *Opt Lett* **20**, 1486–1488.

[35] Bouma BE, Tearney GJ, Bilinsky IP, and Golubovic B (1996). Self phase modulated Kerr-lens mode locked Cr:forsterite laser source for optical coherent tomography. *Opt Lett* **21**, 1839–1841.

[36] Drexler W, Morgner U, Kaertner FX, Pitris C, Boppart SA, Li XD, Ippen EP, and Fujimoto JG (1999). *In vivo* ultrahigh resolution optical coherence tomography. *Opt Lett* **24**, 1221–1223.

[37] Boppart SA, Bouma BE, Pitris C, Southern JF, Brezinski ME, and Fujimoto JG (1998). *In vivo* cellular optical coherence tomography imaging. *Nat Med* **4**, 861–865.

[38] Tearney GJ, Boppart SA, Bouma BE, Brezinski ME, Weissman NJ, Southern JF, and Fujimoto JG (1996). Scanning single-mode fiber optic catheter–endoscope for optical coherence tomography. *Opt Lett* **21**, 912–912.

[39] Boppart SA, Bouma BE, Pitris C, Tearney GJ, Fujimoto JG, and Brezinski ME (1997). Forward-imaging instruments for optical coherence tomography. *Opt Lett* **22**, 1618–1620.

[40] Fujimoto JG, Boppart SA, Tearney GJ, Bouma BE, Pitris C, and Brezinski ME (1999). High resolution *in vivo* intraarterial imaging with optical coherence tomography. *Heart* **82**, 128–133.

[41] Sergeev AM, Gelikonov VM, Gelikonov GV, Feldchtein FI, Kuranov RV, Gladkova ND, Shakhova NM, Snopova LB, Shakov AV, Kuznetzova IA, Denisenko AN, Pochinko VV, Chumakov YP, and Streltzova OS (1997). *In vivo* endoscopic OCT imaging of precancer and cancer states of human mucosa. *Opt Express* **1**, 432.

[42] Feldchtein FI, Gelikonov GV, Gelikonov VM, Kuranov RV, Sergeev A, Gladkova ND, Shakhov AV, Shakova NM, Snopova LB, Terent'eva AB, Zagainova EV, Chumakov YP, and Kuznetzova IA (1998). Endoscopic applications of optical coherence tomography. *Opt Express* **3**, 257.

[43] Kremkau FW (1984). Diagnostic Ultrasound: Principles, Instrumentation, and Exercises (2nd ed). Grune and Stratton, Philadelphia.

[44] Fish P (1990). Physics and Instrumentation of Diagnostic Medical Ultrasound. John Wiley and Sons, New York.

[45] Kremkau FW (1990). Doppler Ultrasound: Principles and Instruments. WB Saunders, Philadelpha.

[46] Zwiebel WJ (1992). Introduction to Vascular Ultrasonography (3rd ed). WB Saunders, Philadelpha.

[47] Erbel R, Roelandt JRTC, Ge J, and Gorge G (1998). Intravascular Ultrasound. Martin Dunitz, London.

[48] Youngquist RC, Carr S, and Davies DEN (1987). Optical coherence-domain reflectometry: a new optical evaluation technique. *Opt Lett* **12**, 158–160.

[49] Takada K, Yokohama I, Chida K, and Noda J (1987). New measurement system for fault location in optical waveguide devices based on an interferometric technique. *Appl Opt* **26**, 1603–1606.

[50] Gilgen HH, Novak RP, Salathe RP, Hodel W, and Beaud P (1989). Submillimeter optical reflectometry. *IEEE J Lightwave Technol* **7**, 1225–1233.

[51] Fercher AF, Mengedoht K, and Werner W (1988). Eye-length measurement by interferometry with partially coherent light. *Opt Lett* **13**, 1867–1869.

[52] Huang D, Wang J, Lin CP, Puliafito CA, and Fujimoto JG (1991). Micron-resolution ranging of cornea and anterior chamber by optical reflectometry. *Lasers Surg Med* **11**, 419–425.

[53] Hee MR, Puliafito CA, Wong C, Duker JS, Reichel E, Schuman JS, Swanson EA, and Fujimoto JG (1995). Optical coherence tomography of macular holes. *Ophthalmology* **102**, 748–756.

[54] Hee MR, Puliafito CA, Wong C, Reichel E, Duker JS, Schuman JS, Swanson EA, and Fujimoto JG (1995). Optical coherence tomography of central serous chorioretinopathy. *Am J Ophthalmol* **120**, 65–74.

[55] Hee MR, Puliafito CA, Wong C, Duker JS, Reichel E, Rutledge B, Schuman JS, Swanson EA, and Fujimoto JG (1995). Quantitative assessment of macular edema with optical coherence tomography. *Arch Ophthalmol* **113**, 1019–1029.

[56] Hee MR, Baumal CR, Puliafito CA, Duker JS, Reichel E, Wilkins JR, Coker JG, Schuman JS, Swanson EA, and Fujimoto JG (1996). Optical coherence tomography of age-related macular degeneration and choroidal neovascularization. *Ophthalmology* **103**, 1260–1270.

[57] Krivoy D, Gentile R, Liebmann JM, Stegman Z, Walsh JB, and Ritch R (1996). Imaging congenital optic disc pits and associated maculopathy using optical coherence tomography. *Arch Ophthalmol* **114**, 165–170.

[58] Lincoff H, and Kreissig I (1998). Optical coherence tomography of pneumatic displacement of optic disc pit aculopathy. *Br J Ophthalmol* **82**, 367–372.

[59] Schaudig U, Hassenstein A, Bernd A, Walter A, and Richard G (1998). Limitations of imaging choroidal tumors *in vivo* by optical coherence tomography. *Graefe's Arch Clin Exp Ophthalmol* **236**, 588–592.

[60] Toth CA, Birngruber R, Boppart SA, Hee MR, Fujimoto JG, DiCarlo CD, Swanson EA, Cain CP, Narayan DG, Noojin GD, and Roach WP (1997). Argon laser retinal lesions evaluated *in vivo* by optical coherence tomography. *Am J Ophthalmol* **123**, 188–198.

[61] Schuman JS, Hee MR, Puliafito CA, Wong C, Pedut-Kloizman T, Lin CP, Hertzmark E, Izatt JA, Swanson EA, and Fujimoto JG (1995). Quantification of nerve fiber layer thickness in normal and glaucomatous eyes using optical coherence tomography. *Arch Ophthalmol* **113**, 586–596.

[62] Schuman JS, and Noecker RJ (1995). Imaging of the optic nerve head and nerve fiber layer in glaucoma. *Ophthalmol Clin No Amer* **8**, 259–279.

[63] Schuman JS, Pedut-Kloizman T, Hertzmark E, Hee MR, Wilkins JR, Coker JG, Puliafito CA, Fujimoto JG, and Swanson EA (1996). Reproducibility of nerve fiber layer thickness measurements using optical coherence tomography. *Ophthalmology* **103**, 1889–1898.

[64] Hee MR, Puliafito CA, Duker JS, Reichel E, Coker JG, Wilkins JR, Schuman JS, Swanson EA, and Fujimoto JG (1998). Topography of diabetic macular edema with optical coherence tomography. *Ophthalmology* **105**, 360–370.

[65] Falk E (1983). Plaque rupture with severe pre-existing stenosis precipitating coronary thrombosis, characteristics of coronary atherosclerotic plaques underlying fatal occlusive thrombi. *Br Heart J* **50**, 127–134.

[66] Davies MJ, and Thomas AC (1983). Plaque fissuring — the cause of acute myocardial infarction, sudden ischemic death, and crescendo angina. *Br Heart J* **53**, 363–373.

[67] Richardson PD, Davies MJ, and Born GVR (1989). Influence of plaque configuration and stress distribution on fissuring of coronary atherosclerotic plaques. *Lancet* **I**, 941–944.

[68] Fuster VL, Badimon L, Badimon JJ, and Chesebro JH (1992). The pathogenesis of coronary artery discease and the acute coronary syndromes. *N Engl J Med* **326**, 242–249.

[69] Loree HM, and Lee R (1992). Stress analysis of unstable plaque. *Circ Res* **71**, 850.

[70] Gillum RF (1989). Sudden coronary death in the United States; 1980–1985. *Circulation* **79**, 756–764.

[71] Nissen SE, Gurley JC, Booth DC, and DeMaria AN (1992). Intravascular ultrasound of the coronary arteries: current applications and future directions. *Am J Cardiol* **69**, 18H–29H.

[72] Lee D-Y, Eigler N, Luo H, Steffen W, Tabak S, and Seigel RJ (1994). Intravascular coronary ultrasound imaging, is it useful? *J Am Coll Cardiol* Suppl., 241A.

[73] Benkeser PJ, Churchwell AL, Lee C, and Aboucinaser DM (1993). Resolution limitations in intravascular ultrasound imaging. *J Am Soc Echocard* **6**, 158–165.

[74] Kimmey MB, Martin RW, Haggitt RC, *et al.* (1989). Histologic correlates of gastrointestinal ultrasound images. *Gastroenterology* **96**, 433–441.

[75] Botet JF, and Lightdale C (1992). Endoscopic ultrasonography of the upper gastrointestinal tract. *Radiologic Clinics of North America* **30**, 1067–1083.

[76] Hawes RH (1993). New staging techniques: endoscopic ultrasound. *Cancer* **71**, 4207–4213.
[77] Furukawa T, Naitoh Y, and Tsukamoto Y (1992). New technique using intraductal ultrasound for diagnosis of diseases of the pancreatobiliary system. *J Ultrasound Med* **11**, 607–612.
[78] Rosh T (1994). Endoscopic ultrasonography. *Endoscopy* **26**, 148–168.
[79] Falk GW, Catalano MF, Sivak MV, Rice TW, and Van Dam J (1994). Endosconography in the evaluation of patients with Barrett's esophagus and high grade dysplasia. *Gastrointest Endosci* **40**, 207–212.
[80] Hizawa K, Suekane H, Aoyagi K, Matsumoto T, Nakamura S, and Fujishima M (1996). Use of endosonographic evaluation of colorectal tumor depth in determining the appropriateness of endoscopic mucosal resection. *Am J Gastroenterol* **91**, 768–771.
[81] Wiersema MJ, and Wiersema LM (1993). High-resolution 25-MHz ultrasonography of the gastrointestinal wall: histologic correlates. *Gastrointestinal Endoscopy* **39**, 499–504.
[82] Yanai H, Tada M, Karita M, and Okita K (1996). Diagnostic utility of 20-megahertz linear endoscopic ultrasonography in early gastric cancer. *Gastrointestinal Endoscopy* **44**, 29–33.
[83] Yanai H, Yoshida T, Harada T, Matsumoto Y, Nishiaki M, and Shigemitsu T (1996). Endoscopic ultrasonography of superficial esophageal cancers using a thin ultrasound probe system equipped with switchable radial and linear scanning modes. *Gastrointestinal Endoscopy* **44**, 578–582.
[84] Boppart SA, Herrmann J, Pitris C, Stamper DL, Brezinski ME, and Fujimoto JG (1999). High-resolution optical coherence tomography-guided laser ablation of surgical tissue. *J Surg Res* **82**, 275–284.
[85] Culbertson JH, Rand RP, and Jurkiewicz MJ (1990). Advances in microsurgery. *Adv Surg* **23**, 57–88.
[86] Wyrick JD, and Stern PJ (1992). Secondary nerve reconstruction. *Microsurgery* **8**, 587–598.